ISSN 2176-5480

22nd International Congress of Mechanical Engineering (COBEM 2013)
November 3-7, 2013, Ribeirão Preto, SP, Brazil

TIME SERIES AND SPECTRAL ANALYSIS OF NONLINEAR AEROELASTIC OSCILLATIONS

Rui Vasconcellos
São Paulo State University, São João da Boa Vista-SP, Brazil
rui.vasconcellos@sjbv.unesp.br
Flávio Marques
Daniel Pereira
Laboratory of Aeroelasticity, Universty of São Paulo, Brazil
fmarques@sc.usp.br

Abstract. *Complex aeroelastic phenomena, such as Limit cycle oscillations, chaos and bifurcations have been observed in wind tunnels tests and real aircrafts. Such phenomenas are related with nonlinear aerodynamic or structural conditions that can be faced by aeroelastic systems. In all these cases, the complex responses of the system are of extreme importance for aircraft safety and performance. In this work, the effects of aerodynamic stall and structural hardening pitch nonlinearities in a two degrees of freedom airfoil are investigated trough numerical integration. The resulting time series are analyzed using time series analysis and Higher Order Spectral analysis in order to characterize the nonlinear couplings between the harmonics generated by the structural stiffness, stall effects and the asymmetry introduced by an offset angle of attack.*

Keywords: *Aeroelasticity, stall, hardening stiffness, LCO, nonlinear couplings.*

1. INTRODUCTION

Characterization of nonlinearities in aircraft is critical to the solution of aeroelastic problems where an optimal relation between performance and safety is desirable. Aeroelastic systems are inherently nonlinear. Nonlinearities can be admitted in the project, or may arise at any time during the life of the aircraft, significantly affecting the predicted response by conventional methods of linear analysis and reducing the limits for catastrophic instabilities (Vasconcellos *et al.*, 2012; Conner *et al.*, 1996; Fung, 1993; Lee *et al.*, 1997; Li *et al.*, 2010). Therefore, it is important to characterize, identify and include such non-linear effects to the design and development of aircraft. Common aeroelastic nonlinear phenomena, such as Limit cycle oscillations, chaos and bifurcations have been observed in wind tunnels tests and real aircrafts. Such phenomenas are related with nonlinear aerodynamic or structural conditions that can be faced by aeroelastic systems. Aerodynamic nonlinearities can occur for instance, in transonic flight and high angles of attack attitudes (Ericsson and Reding, 1987; Lee *et al.*, 1999; Dowell and Tang, 2002). In terms of structural properties, the effects of aging, loose attachments, material features, large motions or deformations are examples of non-linearities to be considered. In all these cases, the complex responses of the system are of extreme importance for aircraft safety and performance. Sometimes a nonlinearity has the effect of initiating instability, but it also possible for a nonlinear effect to limit the response in an otherwise dangerous situation. In addition, recently, stable aeroelastic nonlinear oscillations becomes desired for aeroelastic energy harvesting purposes. In this work, the combined effects of concentrated structural nonlinearities and stall effects in a two degrees of freedom airfoil are investigated for structural hardening pitch, under influence of relatively large angle of attack oscillations, leading to stall conditions. All the analysis are based in numerical integration of a typical section model, with modified Theodorsen unsteady aerodynamics to incorporate stall effect, similar as did in the work of Gilliatt *et al.* (1998) for quasi-steady approach of Theodorsen function. The resulting time series and phase portraits will be analyzed and Higher Order Spectral analysis will be performed in order to characterize the nonlinear couplings between the harmonics generated by the nonlinear terms.

Higher-order spectral analysis can be used to detect and identify nonlinear coupling between frequency modes in a time series. Higher-order spectral moments are multidimensional Fourier transforms of higher-order statistics. The basis for the use of *HOS* in the detection of nonlinear coupling among frequency modes is that if two frequency components (f1 and f2) and their sum components (f1 and f2) are coupled in a time series through a quadratically nonlinear interaction mechanism, phase coherence will exist among them. Under these conditions, the averaging will lead to a large value of the autobispectrum. Similarly, the cubic interaction of three frequency components (f1, f2, and f3) yields a large value for the autotrispectrum (Hajj and Beran, 2008).

2. Nonlinear Aeroelastic Model

The aeroelastic system consists of a two-dimensional airfoil that has two degrees of freedom including pitch and plunge motions. The plunge and pitch motions are measured at the elastic axis which are denoted by h and α, respectively. The

ISSN 2176-5480

Table 1: Concentrated typical section parameters of the aeroelastic wing

$span$	Wing span (m)	0.5
b	Wing semi-chord (m)	0.125
a	Position of elastic axis relative to the semi-chord	-0.5
ρ_p	Air density (kg/m^3)	1.1
m_w	Mass of the wing (kg)	1.716
m_T	Mass of wing and supports (kg)	3.53
r_α^2	radius of gyration square (kgm^2)	0.53
ω_α	natural frequency of pitch (rad/s)	17.16
ω_h	natural frequency of plunge (rad/s)	30.72
x_α	Nondimensional distance between center of gravity and elastic axis	0.66

distance from the elastic axis to mid-chord is represented by ab where a is a constant and b is the semi-chord length of the entire airfoil section. The mass center of the entire airfoil is located at a distance $x_\alpha b$ from the elastic axis. The two spring forces for plunge and pitch are represented by k_h and k_α, respectively. The viscous damping forces are described through the coefficients c_h and c_α for plunge and pitch, respectively. Finally, U is used to denote the freestream velocity. Using Lagrange's equations, the equations of motion governing this system are written as:

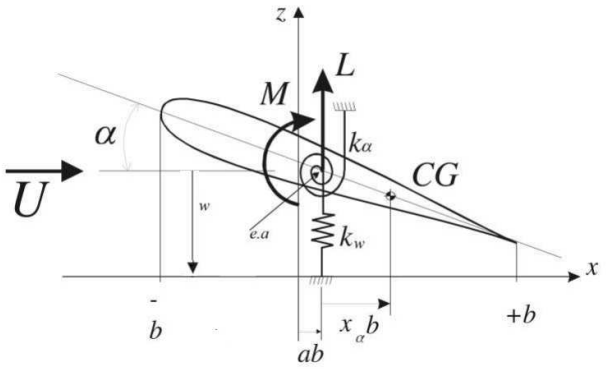

Figure 1: Schematic of an aeroelastic system under uniform airflow

$$\begin{bmatrix} m_T & m_w x_\alpha b \\ m_w x_\alpha b & I_\alpha \end{bmatrix} \begin{bmatrix} \ddot{h} \\ \ddot{\alpha} \end{bmatrix} + \begin{bmatrix} c_h & 0 \\ 0 & c_\alpha \end{bmatrix} \begin{bmatrix} \dot{h} \\ \dot{\alpha} \end{bmatrix} + \begin{bmatrix} k_h & 0 \\ 0 & k_\alpha F(\alpha)/\alpha \end{bmatrix} \begin{bmatrix} h \\ \alpha \end{bmatrix} = \begin{bmatrix} -L \\ M \end{bmatrix} \tag{1}$$

where m_T is the mass of the entire system (wing and support), m_w is the wing mass alone, I_α is the mass moment of inertia about the elastic axis. The values of these parameters used in the following analysis are given in Table 1. In addition, L and M are the aerodynamic lift and moment about the elastic axis. $F(\alpha)$ is a function used to represent the pitch nonlinearity in the system.

The function $F(\alpha)$ has the effect of a hardening pitch, and can be used to introduce an offset angle of attack by changing the term a_0 in the $F(\alpha)$ equation, given by:

$$F(\alpha) = a_0 + a_3\alpha^3 \tag{2}$$

This feature is shown in 2 as obtained by using Eq. (2)

3. Representation of the aerodynamic loads

The aerodynamic loads are modeled using Theodorsen approach Theodorsen (1935), where the unsteady aerodynamic forces and moments are written respectively as:

$$L = \pi\rho b^2 \left[\ddot{h} + U\dot{\alpha} - ba\ddot{\alpha}\right] + 2\pi\rho UbQC + G(\alpha) \tag{3}$$

ISSN 2176-5480

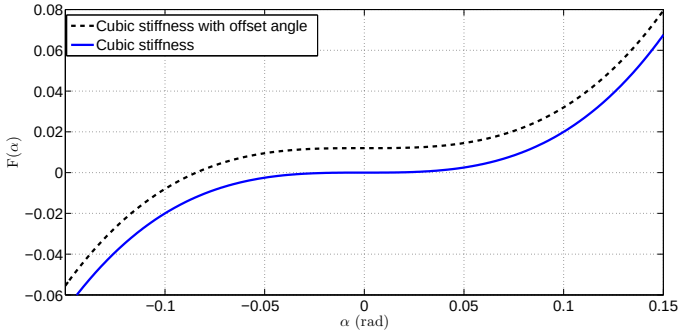

Figure 2: Pitch angle *versus* torque described in Eq. (2), for $a_3 = 20$, $a_0 = 0$ and $a_0 \neq 0$

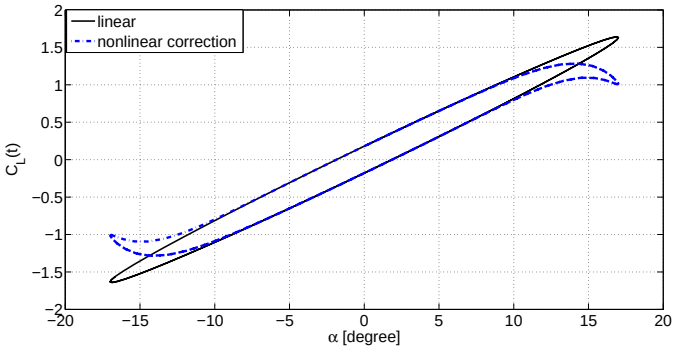

Figure 3: Lift coefficient versus angle of attack using Theodorsen function (continuous) and using the modified version (discontinuous) with $G(\alpha)$

and

$$M_\alpha = \pi\rho b^2 \left[ba\ddot{h} - Ub\left(\frac{1}{2} - a\right)\dot{\alpha} - b^2\left(\frac{1}{8} + a^2\right)\ddot{\alpha}\right] + 2\pi\rho b^2 U(a + \frac{1}{2})QC \tag{4}$$

where U is the freesteram velocity, C is the Theodorsen function, and

$$Q = U\alpha + \dot{h} + \dot{\alpha}b\left(\frac{1}{2} - a\right) \tag{5}$$

The function $G(\alpha)$ in Equation(3) introduce the nonlinear effect of stall. For this analysis, it is given by:

$$G(\alpha) = g_0 + g_7\alpha^7 \tag{6}$$

The effect of $G(\alpha)$ in the $C_L vs.\ \alpha$ plot is shown in figure 3.

The aerodynamic loads given in Eqs. (3) and (4) depend on Theodorsen function $C(k)$, where $k = \frac{\omega b}{U}$ is the reduced frequency of harmonic oscillations. Considering the unsteady effect in the flow, the aerodynamic loads associated with Theodorsen function can be manipulated by convolution based on Duhamel formulation in the time domain Edwards *et al.* (1979); Trickey *et al.* (2002); Vasconcellos *et al.* (2012). Using the Sears and Pade approximations, the unsteady representation of the aerodynamic loads are modeled as follows Abdelkefi *et al.* (2012):

$$L = \pi\rho b^2\left[\ddot{h} + U\dot{\alpha} - ba\ddot{\alpha}\right] + 2\pi\rho Ub(c_0 - c_1 - c_3)Q + 2\pi\rho U^3 c_2c_4(c_1 + c_3)\bar{x} + 2\pi\rho U^2 b(c_1c_2 + c_3c_4)\dot{\bar{x}} + G(\alpha) \tag{7}$$

and

$$\begin{aligned} M_\alpha = \pi\rho b^2\left[ba\ddot{h} - Ub\left(\frac{1}{2} - a\right)\dot{\alpha} - b^2\left(\frac{1}{8} + a^2\right)\ddot{\alpha}\right] + 2\pi\rho b^2 U(a + \frac{1}{2})(c_0 - c_1 - c_3)Q \\ +2\pi\rho bU^3(a + \frac{1}{2})c_2c_4(c_1 + c_3)\bar{x} + 2\pi\rho b^2U^2(a + \frac{1}{2})(c_1c_2 + c_3c_4)\dot{\bar{x}} \end{aligned} \tag{8}$$

where $c_0 = 1$, $c_1 = 0.165$, $c_2 = 0.0455$, $c_3 = 0.335$, and $c_4 = 0.3$. These coefficients are present due to the Sears approximation to the Wagner function. $\bar{x}$ and $\dot{\bar{x}}$ are two augmented variables in the state space. They are related to the system variables by the following second-order differential equation:

$$\ddot{\bar{x}} = -c_2c_4\frac{U^2}{b^2}\bar{x} - (c_2 + c_4)\frac{U}{b}\dot{\bar{x}} + \frac{U}{b}\alpha + (\frac{1}{2} - a)\dot{\alpha} + \frac{\dot{h}}{b} \tag{9}$$

ISSN 2176-5480

More details for the derivation of the aerodynamic loads based on the Duhamel formulation can be found in Abdelkefi et al. Abdelkefi *et al.* (2012).

4. NONLINEAR RESULTS

The simulations were carried out for two defined conditions. The first one is for a typical section with symmetric cubic stiffness. As the wind speed increases, the system cross the linear flutter boundary and start to oscillate in a Limit Cicle Oscillation (LCO) induced by the hardening stiffness. At the beginning, the oscillations has relatively low amplitudes, but as the speed increase, the amplitudes start to become large enough and the system faces stall effects.

In the second condition, the wing is positioned with an offset angle of attack. Again the amplitudes at the beginning are relatively low, but at higher speeds, the stall effects appears.

4.1 Condition 1: Symmetric hardening

In this condition, the term a_0 in Equation 2 is set to zero. The flutter speed for this system is around 8.7m/s. The behavior will be analyzed for two speeds, the first one just after the flutter (at 8.8m/s) and for higher speed (15m/s).

Figure 4 present the time series at 8.8m/s. is possible to observe limited amplitude oscillations with a subharmonic component and the maximum amplitude around 12 degrees.

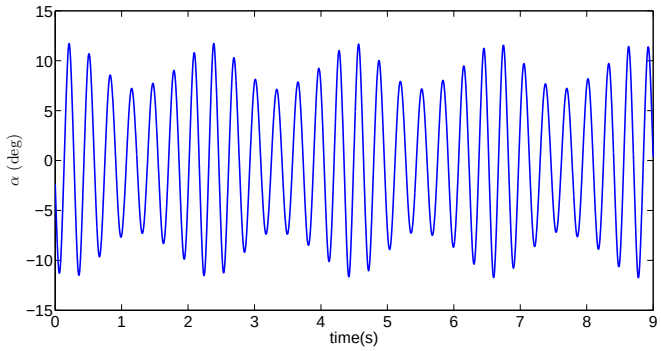

Figure 4: Time series of angle of attack at 8.8m/s and symmetric hardening

Figures 5 present the phase portrait and the power spectrum for this first configuration, as can be observed, the cubic harmonic is present, with sidebands around the main peaks.

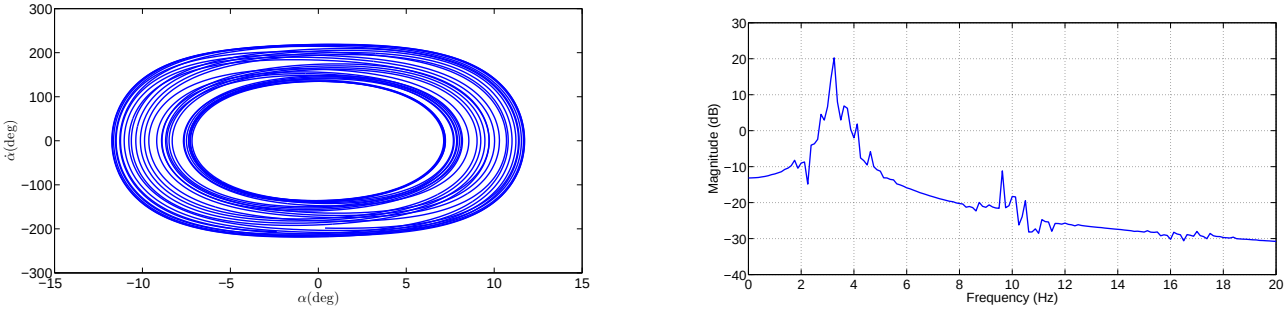

(a) (b)

Figure 5: (a) Phase portrait and (b) Power spectrum with symmetric hardening at 8.8m/s

The same analysis follows to a speed of 15m/s. Figure 6 present the time series at 15m/s. is possible to observe higher amplitudes and a overall change in behavior.

Figures 7 present the phase portrait and the power spectrum for this second configuration.

One can observe that stronger super-harmonics show up when the speed is higher, but also, some quadratic terms appear in figure 7(b) around $6Hz$ and $12Hz$.

4.2 Condition 2: Offset angle and hardening

In this condition, the term a_0 in Equation 2 is set to introduce an offset angle of 5 degrees. Again, the behavior will be analyzed for two speeds, the first one just after the flutter (at 8.8m/s) and for higher speed (15m/s).

ISSN 2176-5480

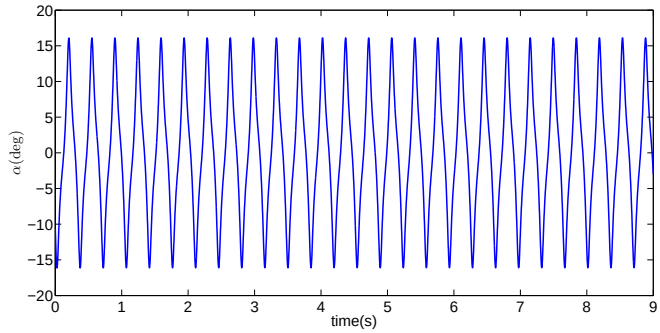

Figure 6: Time series of angle of attack at 15m/s and symmetric hardening

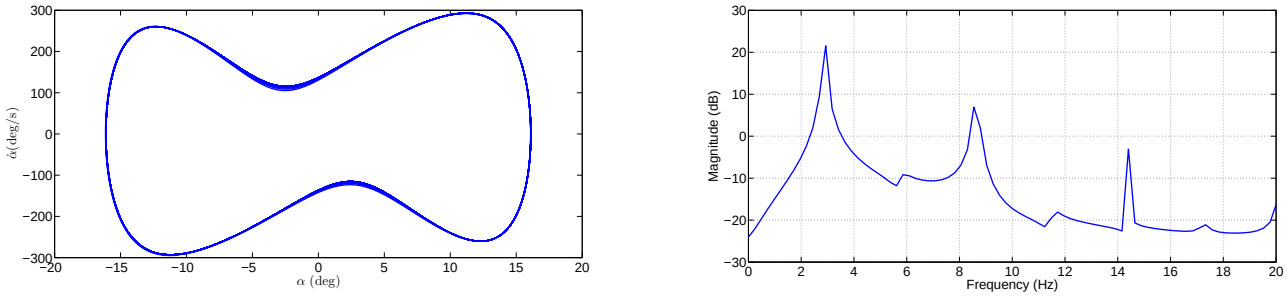

(a) (b)

Figure 7: (a) Phase portrait and (b) Power spectrum with symmetric hardening at 15m/s

Figure 8 present the time series at 8.8m/s. Again, is possible to observe limited amplitude oscillations with a subharmonic component and the asymmetric amplitude between around -12 degrees and 10 degrees.

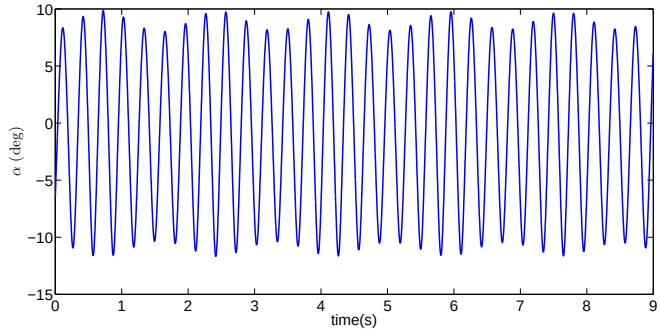

Figure 8: Time series of angle of attack at 8.8m/s with 5 deg. offset angle and hardening

Figures 9 present the phase portrait and the power spectrum for this first speed.

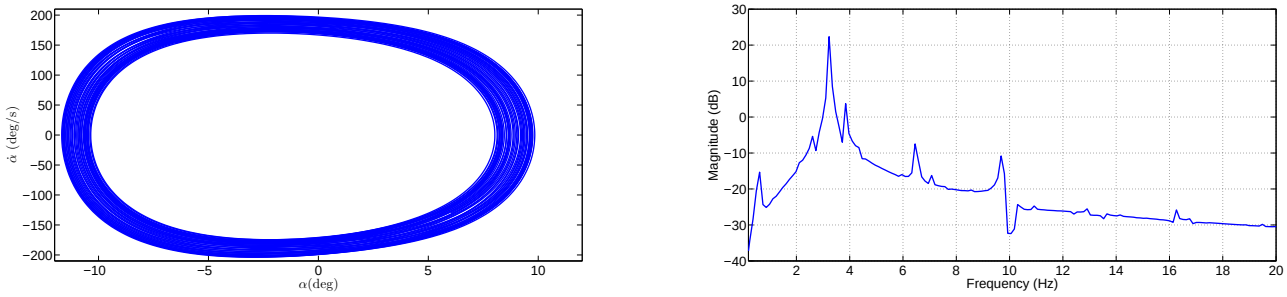

(a) (b)

Figure 9: (a) Phase portrait and (b) Power spectrum with 5 deg. offset angle and hardening at 8.8m/s

The same analysis follows to a speed of 15m/s. Figure 10 present the time series at 15m/s. is possible to observe

ISSN 2176-5480

higher amplitudes and a well defined change in behavior.

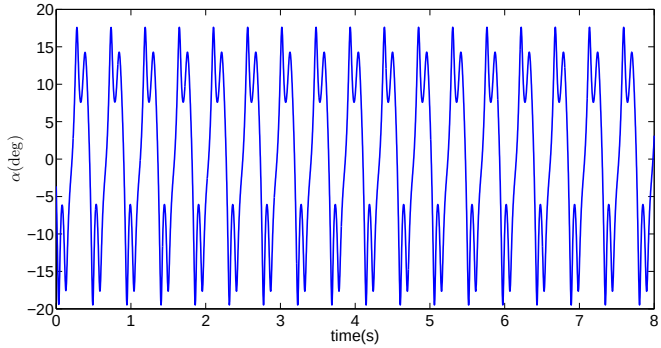

Figure 10: Time series of angle of attack at 15m/s with 5 deg. offset angle and hardening

Figures 11 present the phase portrait and the power spectrum for this second configuration.

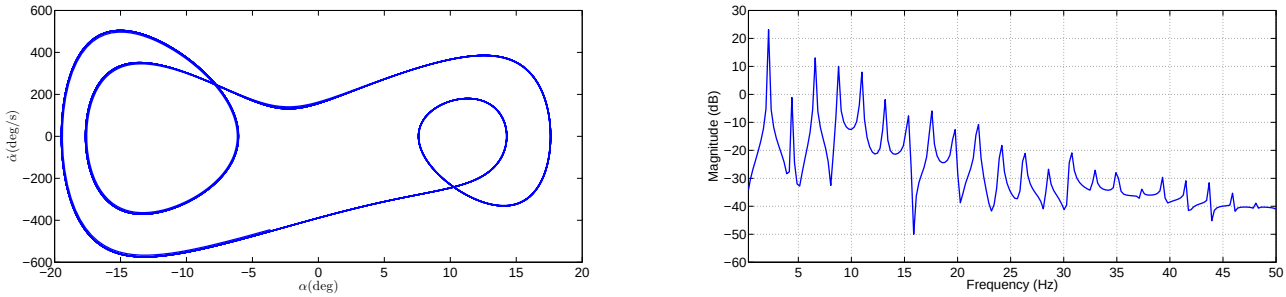

(a) (b)

Figure 11: (a) Phase portrait and (b) Power spectrum with 5 deg. offset angle and hardening at 15m/s

Is possible to observe strong harmonic generation as consequence of the offset angle and the higher amplitudes reached by the system in figure 11(b). These harmonic generation are result of the nonlinear couplings between different internal frequencies.

4.3 Higher order Spectral analysis -(HOS)

The autobicoherence is now applied for the Condition 2, with offset angle hardening at tree different speeds, in order to visualize the evolution of the nonlinear quadratic couplings with freestream increase.

As observed in figure 12, nonlinear quadratic coupling exist at all tree investigated speeds. For the first investigated speed, namely, 8.8m/s, is possible to observe couplings between the main frequency (aroud 3,25Hz) and its quadratic and cubic harmonics (6,5Hz and 9,75Hz) in figure 12(a). As the speed increases and as a result of harmonic couplings, new harmonics and subharmonics are generated, increasing the number of frequencies in the system, as observed in figures 12(b) and 12(c). Is is expected that for higher speeds, more frequencies will be generated, resulting in a broadband spectrum and this system will probably become chaotic.

5. CONCLUDING REMARKS

The effects of a symmetric and asymmetric hardening pitch nonlinearity in a pitch/plunge typical section at high angle of attack were investigated in this work. It was found that the combination of asymmetric pitch and stall effect can lead to a very complex scenario of nonlinear aeroelastic oscillations with several nonlinear couplings between natural frequencies, subharmonics and superharmonics, with increase of actuating frequencies as freestream speed increases. Further analysis are planned for experimental validation of observed results and to explore the system at higher speeds, where probably chaotic behavior will take place.

6. ACKNOWLEDGEMENTS

The authors acknowledge the financial support of the São Paulo State Research Agency, FAPESP, Brazil (grant 2012/08459-1)

ISSN 2176-5480

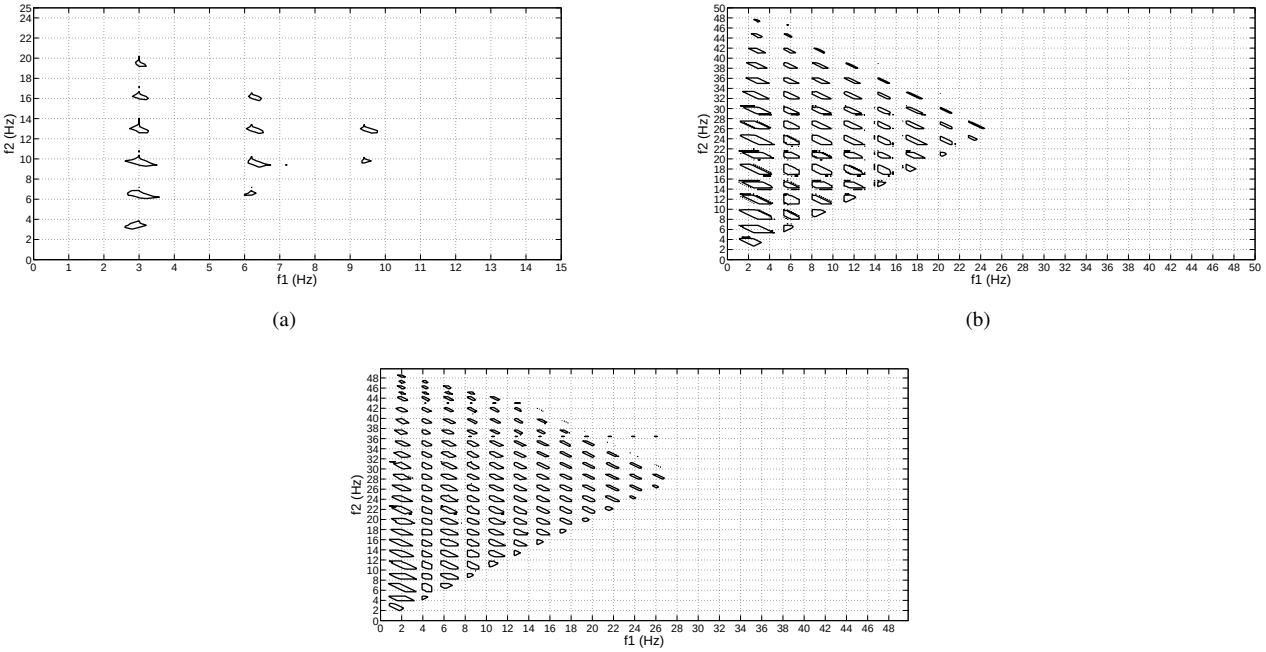

Figure 12: Auto-bicoherence contour plot (level 0.99) at (a) 8.8m/s (b) 13m/s and (c) 15m/s

7. REFERENCES

Abdelkefi, A., Vasconcellos, R., Nayfeh, A.H. and Hajj, M.R., 2012. "An analytical and experimental investigation into limit-cycle oscillations of an aeroelastic system". *Nonlinear Dynamics*, Vol. 71, pp. 159–173.

Conner, M.D., Tang, D.M., Dowell, E.H. and Virgin, L.N., 1996. "Nonlinear behavior of a typical airfoil section with control surface freeplay". *Journal of Fluids and Structures*, , No. 11, pp. 89–109.

Dowell, E. and Tang, D., 2002. "Nonlinear aeroelasticity and unsteady aerodynamics". *AIAA Journal*, Vol. 40, No. 9, pp. 1187–1196.

Edwards, J.W., Ashley, H. and Breakwell, J.V., 1979. "Unsteady aerodynamic modeling for arbitrary motions". *AIAA J.*, Vol. 17, pp. 365–374.

Ericsson, L. and Reding, J., 1987. "Fluid dynamics of unsteady separated flow. Part II: Lifting surfaces". *Progress in Aerospace Sciences*, Vol. 24, pp. 249–356.

Fung, Y.C., 1993. *An introduction to the theory of Aeroelasticity*. New York: Dover Publications.

Gilliatt, H.C., Strganac, T.W. and Kurdila, A.J., 1998. "On the presence of internal resonances in aeroelastic systems".

Hajj, M.R. and Beran, P., 2008. "Higher-order spectral analysis of limit cycle oscillations of fighter aircraft". *Journal of Aircraft*, Vol. 45, No. 6.

Lee, B.H.K., Gong, L. and Wong, Y.S., 1997. "Analisys and computation of nonlinear dynamic response of a two degree of freedom system and its application in aeroelasticity". *Journal of Fluids and Structures*, Vol. 11, pp. 225–246.

Lee, B.H.K., Price, S. and Wong, Y., 1999. "Nonlinear aeroelastic analysis of airfoils: bifurcation and chaos". *Progress in Aerospace Sciences*, Vol. 35, No. 3, pp. 205–334.

Li, D., Guo, S. and Xiang, J., 2010. "Aeroelastic dynamic response and control of an airfoil section with control surface nonlineatities". *Journal of Sound and Vibration*, , No. 329, pp. 4756–4771.

Theodorsen, T., 1935. "General theory of aerodynamic instability and the mechanism of flutter". Technical Report 496, NACA.

Trickey, T., Virgin, L.N. and Dowell, H., 2002. "The stability of limit-cycle oscillations in an nonlinear aeroelastic system". *Proceedings: Mathematical, Physical and Engineering Sciences*, Vol. 458, No. 2025, pp. 2203–2226.

Vasconcellos, R., Abdelkefi, A., Marques, F.D. and Hajj, M.R., 2012. "Representation and analysis of control surface freeplay nonlinearity". *Journal of Fluids and Structures*, Vol. 31, pp. 79–91. doi:10.1016/j.jfluidstructs.2012.02.003.

8. RESPONSIBILITY NOTICE

The authors are the only responsible for the printed material included in this paper.